Synthetic Metals 162 (2012) 1930–1935

Contents lists available at SciVerse ScienceDirect

Synthetic Metals

journal homepage: www.elsevier.com/locate/synmet

Enhanced carrier extraction efficiency in organic solar cells with reduced space-charge limited transport by engineered vertical compositional profile

Ming-Kun Lee[a], Tsung-Han Kuo[b], Kuo-Wen Kong[a], Yun-Ru Hong[b], Jen-Chun Wang[c], Sheng-Fu Horng[a,*], Hsin-Fei Meng[d]

[a] Department of Electrical Engineering, National Tsing Hua University, Hsinchu 300, Taiwan, ROC
[b] Institute of Photonics Technologies, National Tsing Hua University, Hsinchu 300, Taiwan, ROC
[c] Department of Materials Science and Engineering, National Tsing Hua University, Hsinchu 300, Taiwan, ROC
[d] Institute of Physics, National Chiao Tung University, Hsinchu 300, Taiwan, ROC

ARTICLE INFO

Article history:
Received 1 May 2012
Received in revised form 25 August 2012
Accepted 12 September 2012
Available online 13 October 2012

Keywords:
Polymer solar cells
Space-charge limited effect
Fillfactor
Layer thickness
Light bias
Quantum efficiency

ABSTRACT

A multi-layered polymer solar cell (PSC) with a graded compositional profile to reduce space-charge limited (SCL) transport was designed and analyzed in details. We found that by increasing the effective carrier lifetime for the slower photo-carriers, SCL effects that degrade the fill factor and the power conversion efficiency can be alleviated in PSCs with a thick active layer. The reduction of SCL effects was evidenced by a diminished dependence of the incident photon-to-electron conversion efficiency (IPCE) on light bias, which also indicates the importance of light bias in characterizing the operating IPCE of PSCs with thick active layers which operate in SCL region. Based on our results, device architecture to enhance FF was proposed.

1. Introduction

Polymer solar cells (PSCs) have attracted much attention as potential renewable energy sources because of their advantages of light weight, low fabrication cost, flexibility, and easy manufacturing [1,2]. Conventional PSCs generally comprise a bulk-heterojunction (BHJ) with interpenetrating network of donor (D) and acceptor (A) that gives more interfaces, at which the photo-generated excitons can be efficiently dissociated, yielding a high photo-carrier generation efficiency. Much progress has been made and the power conversion efficiency (PCE) of BHJ PSCs based on poly(3-hexylthiophene) (P3HT) and fullerene derivative (6,6)-phenyl C61 butyric acid methyl ester (PCBM) was reported to exceed 5% [3–5].

The constituting materials in conventional BHJ devices usually exhibit low intrinsic carrier mobility. In addition, the disrupting (discontinuous) nature of donor and acceptor distribution in BHJ layer severely retards the carrier transport. As a result, the BHJ layers were characterized by lower charge-carrier mobilities and low characteristic charge collection lengths [6]. According to the model proposed by Goodman and Rose [7], when the charged carrier mobilities are unbalanced and the blend layer thickness is larger than the characteristic charge collection length, space-charge limited (SCL) transport will be the dominant transport mechanism of the photo-carriers in the BHJ. This leads to a one-half power photocurrent vs. effective voltage (J_{ph}–V_{eff}) relationship around the operating point of the BHJ solar cells, reducing the change in the photocurrent with respect to applied voltage, and the fill factor (FF) as well. Although various methods have been proposed to enhance the P3HT ordering, and thus to improve the balance in carrier mobilities [3,4,8,9], the resulted vertical composition gradient of PCBM and P3HT in the BHJ is unfavorable for the charge extraction [10]. Therefore, there is a tradeoff between the FF and blend layer thickness, which is related to absorption, for conventional BHJ solar cells. Although the use of high mobility materials [11] and modified cathode structure with interlayer [12,13] help reduce the SCL effects, the use of conventional and well-known materials is still advantageous to elucidate the origin of FF degradation. In this paper, we proposed a scheme to reduce the SCL effect in BHJ solar cells by introducing a P3HT-rich layer between the active blend layer and the bottom anode. We found that the SCL effects can indeed be reduced, leading to an enhanced FF. Our results thus suggest the possibility to increase the absorption layer thickness while maintaining a high FF.

* Corresponding author. Tel.: +886 3 5715131x42578; fax: +886 3 5752120.
E-mail addresses: sfhorng@ee.nthu.edu.tw, d945016@oz.nthu.edu.tw (S.-F. Horng).

0379-6779/$ – see front matter © 2012 Elsevier B.V. All rights reserved.
http://dx.doi.org/10.1016/j.synthmet.2012.09.007

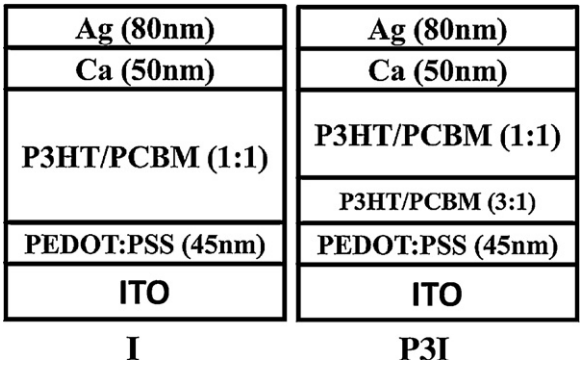

Fig. 1. Layer structure for device P3I and I used in this study.

According to Goodman and Rose [7], the photocurrent (J_{ph}) due to double extraction of electron–hole pairs from devices with non-injecting contacts at low effective voltage (V_{eff}) is given by

$$J_{ph} = \frac{gel[1+b]}{b}\left(\frac{V_{eff}\tau_s\upsilon_s}{l^2}\right) \quad (1)$$

where g, e, l, τ_s, and υ_s denote the photo-carrier generation rate, the electronic charge, the layer thickness, the lifetime and the mobility of slow carriers, respectively, and $b = \tau_s\upsilon_s/\tau_f\upsilon_f$ is the ratio of the product of carrier mobility and lifetime of slow carriers to that of fast carriers. Since the contacts for practical organic photovoltaic devices are not completely non-injecting, we follow Blom et al. to reduce phenomenally the carrier injection by subtracting the measured illuminated current (J_{light}) from the measured dark current (J_{dark}) [14]. The photocurrent (J_{ph}) and the effective voltage (V_{eff}) in Eq. (1) are thus given by $J_{ph} = J_{dark} - J_{light}$ and $V_{eff} = V_0 - V$, respectively, where V_0, the compensation voltage in [11], is the applied voltage (V) at which J_{dark} equals J_{light}.

At higher V_{eff}, or equivalently at V lower than open-circuit voltage (V_{oc}), the J–V characteristic exhibits a transition to a one-half power law of the effective voltage due to SCL effects, and the transition voltage is given by

$$v_{tr} = \frac{l^2b^2}{4(1-b)\tau_s\upsilon_s} \quad (2)$$

At even higher V_{eff}, which corresponds to reverse applied bias, all photo-carriers are extracted from the active layer. A saturated photocurrent which is independent of voltage will result. The saturated photocurrent is given by

$$J_{ph} = egl \quad (3)$$

In order for the FF to increase, the half-power region needs to be reduced, requiring a larger b in Eq. (2). One way to increase the b is to increase the effective carrier lifetime for the slow photo-carriers. Since the photo-carrier recombination in PSCs follows Langevin recombination, an increased effective carrier lifetime can be achieved by reducing the concentration of the other type of carriers. We therefore add between the active blend layer and the bottom anode a P3HT-rich layer, within which the electron concentration, and thus the recombination as well, is reduced. The weight ratio of P3HT and PCBM for the P3HT-rich layer is 3:1 and that of the active layer for the control device is 1:1. The structures for the control device (I) and the device with insertion of P3HT-rich layer (P3I) are shown in Fig. 1. This layer structure for device P3I is similar to that investigated by Liang et al. [15], albeit with the P3HT electron blocking layer replaced by a P3HT-rich layer inserted for reduced carrier recombination. However, as will be analyzed in details in what follows, our device will operate differently due to the thicker active layer.

2. Experiment

The devices (I and P3I) were prepared as follows. Indium tin oxide (ITO) coated glass was cleaned by acetone and isopropanol to remove residual organic materials. UVO treatment for more hydrophilic surface followed. Hole transporting material, PEDOT:PSS (AI4083), was spun on ITO substrates with a thickness of 45 nm. The device was heated on a hotplate at 200 °C for 5 min in air for a dried film. We then loaded the PEDOT-coated ITO substrates into a glove box in nitrogen ambient. For device P3I, a mixed solution of P3HT and PCBM (P3HT:PCBM = 3:1 in weight) in toluene with a P3HT concentration of 8.5 mg/ml was spun at 3000 rpm for 30 s to achieve a P3HT-rich layer of 70 nm thickness. Toluene rather than more commonly employed 1,2-dicholobezene (DCB) was used in this work since it is more compatible with the fabrication process of the buffer layer technique [16] which we used to circumvent the interlayer mixing problem.

The device was annealed on a hotplate at 140 °C for 10 min to remove the residual solvent and to make it more resistant against the interlayer mixing. Following [16], after spinning the 1,2-propylene glycol as buffer liquid, solution which consists of P3HT and PCBM at weight ratio of 1:1 in toluene with a P3HT concentration of 17 mg/ml, was spun at 1000 rpm for 30 s on the liquid surface immediately to form a multi-layered device (device P3I) with a total active layer thickness of 300 nm. The film was annealed again on a hotplate at 140 °C for 10 min. For the single-layered control device (device I), which consisted of only a blending layer of P3HT and PCBM with weight ratio of 1:1, solution which consists of P3HT and PCBM at weight ratio of 1:1 in toluene with a P3HT concentration of 17 mg/ml, was spun at 550 rpm for 30 s, a condition which was optimized to achieve an equal active layer thickness (300 nm) for both devices. A heat treatment was then carried out on a hotplate at 140 °C for 20 min, which equals the total annealing time for the multi-layered device. Subsequently, a top metal electrode consisting of calcium (50 nm) and silver (80 nm) was thermally deposited under a pressure of 2.3×10^{-6} Torr. The area of active device with the deposited top electrode was 4 mm^2.

3. Characterization

The J–V characteristics of the devices were measured with a Keithley 2400 source measurement unit using a 100 mW/cm^2 AM 1.5G solar simulator (San-ei Electric, XES-301S). The intensity of the incident solar illumination was calibrated by a silicon photodiode (HAMAMATSU S1337-BR). The light intensity was reduced by neutral density filters (Thor lab) to achieve different illumination levels. The incident photon-to-electron conversion efficiency (IPCE) was conducted using a measurement system (model QE-R) built by Enli Technology Co., Ltd. Wide-spectrum light source was chopped and diffracted into separated monochromatic narrow bands, and each of which was projected onto the device under testing. Another wide-spectrum light source was used as optional light bias. The photocurrent generated by incident monochromatic light was converted and amplified to an AC voltage by a trans-impedance amplifier, which was then measured by a DAQ card (National Instrument) at the chopper frequency.

4. Results and discussion

The absorption spectra for active layer of both devices (I and P3I) are shown in Fig. 2. Because the thickness of the active layer for both devices is identical, the absorption spectra nearly

Table 1
The device parameters including J_{sc}, V_{oc}, FF, PCE, V_{max}, J_{max} and V_0 for devices P3I and I.

	J_{sc} (mA/cm^2)	V_{oc} (v)	FF (%)	PCE (%)	V_{max} (v)	J_{max} (mA/cm^2)	V_0 (v)
P3I	9.96	0.63	48.8	3.12	0.46	6.78	0.74
I	9.01	0.63	41.6	2.35	0.42	6.59	0.675

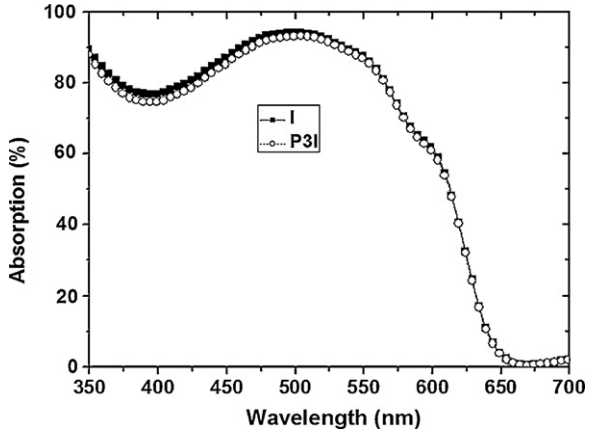

Fig. 2. The absorption spectrum of the active layer for device P3I and I.

overlap as expected. Fig. 3(a) shows the measured dark current density (J_{dark}) and the illuminated current density (J_{light}) as a function of applied voltage (V) for both devices under simulated AM1.5G light illumination at 100 mW/cm^2. In addition, the compensation voltages (V_0) for both devices are labeled. The photovoltaic parameters for both devices are summarized in Table 1. From Table 1, the insertion of the P3HT-rich layer in device P3I has a little effect on V_{oc}, as compared to device I. This is not surprising since V_{oc} depends either on the electrode metal work function or the donor/acceptor energy levels, which are all identical for both devices. However, the short-circuit current density J_{sc} (FF) increases by approximately 10.5% (17.3%) from 9.01 mA/cm^2 (41.6%) to 9.96 mA/cm^2 (48.8%), yielding an improved PCE by 32.3% from 2.35% to 3.12%. Since the absorption remains unchanged (Fig. 2) for both devices, the improvements should arise from the enhanced carrier extraction efficiency. From Fig. 3(a), the dark current density of device P3I is more than that of device I at forward bias, revealing that the carrier injection from the electrode is not suppressed for device P3I as compared to device I. In addition, the dark current density of device P3I shows an order of magnitude higher than that of device I. The reason of this increase in dark current may be attributed to the buffer layer process in which high-boiling point (188 °C) 1,2-propylene glycol buffer was used to circumvent the interlayer mixing problem in preparing device P3I. The residual 1,2-propylene glycol after the annealing (at 140 °C) seems to act as chemical dopants and increases the reverse dark current. A more balanced injection which enhances the recombination among the injected carriers may also play a role. Therefore the improved carrier extraction efficiency for device P3I should not be attributed to suppressed carrier injection, which can causes loss in photocurrent due to the recombination between the photo-carriers and the injected carriers.

For better comparison, the dark current density (J_{dark}) vs. applied voltage (V) characteristics for both devices are plotted in semi-log scale in Fig. 3(b). It is clear that, while there is only slight difference between the current for both devices at forward bias, the dark current of device P3I is higher than that of device I by an order of magnitude at reverse bias. This is different from what was observed in [15], in which the dark current is suppressed at reverse bias by the inserted P3HT electron blocking layer. The absence of suppressed carrier injection from the ITO anode can be understood by noting that the inserted P3HT-rich layer in our device (P3I) consists of PCBM, which allows for electron transport. Our inserted P3HT-rich layer, however, reverts the conventionally observed unfavorable composition profile, which exhibits a higher concentration of PCBM at the ITO side, to a favorable one that facilitates carrier collection. In addition, as will be shown in what follows, the insertion of a P3HT-rich layer reduces carrier recombination. Therefore, increased J_{sc} was obtained even though the absorption remained unchanged.

The photocurrent densities (J_{ph}) vs. effective voltage (V_{eff}) in log–log scale are plotted in Fig. 4 and the maximum power points, V_{max} and I_{max} in Table 1, are also marked. We also include in Fig. 4 auxiliary lines with slope 1 (0.5), which represent balanced (SCL) transport for photo-carriers. As shown in Fig. 4 the SCL dominated region, which follows the auxiliary line of slope 0.5, is narrower for device P3I than that for device I. Since the maximum power points are located in the SCL region, V_{max} and I_{max} for device P3I are larger than those for device I (Fig. 4). The improvement in PCE and FF for device P3I is thus attributed to reduce SCL effects with the insertion of the P3HT-rich layer. It is also notable that current saturation at high effective voltage, which represents the photo-carrier generation rate in Eq. (3) [7], is observed for both devices and the saturation photocurrent densities are 12.5 mA/cm^2 and 12 mA/cm^2

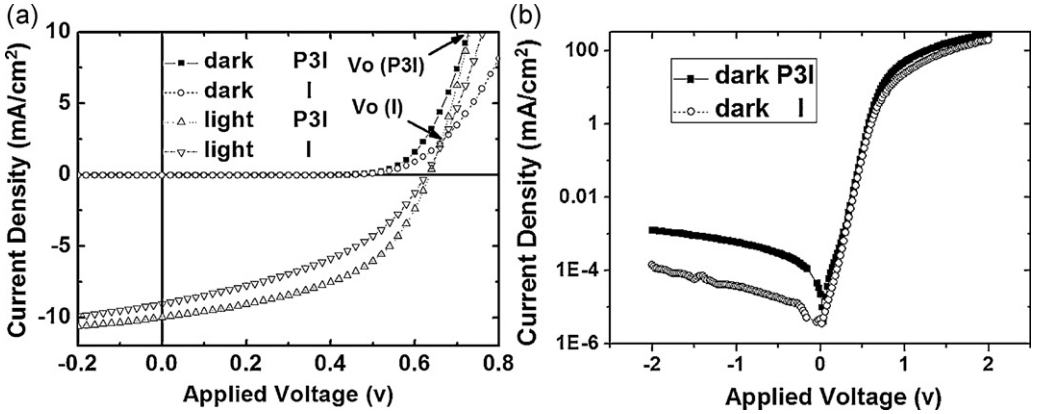

Fig. 3. (a) The illuminated current density (J_{light}) under AM1.5G at 100 mW/cm^2 and dark current density (J_{dark}) vs. voltage (V) for device P3I and I. The compensation voltage (V_0) is labeled for device P3I and I; (b) J_{dark}–V characteristics plotted in semi-log scale.

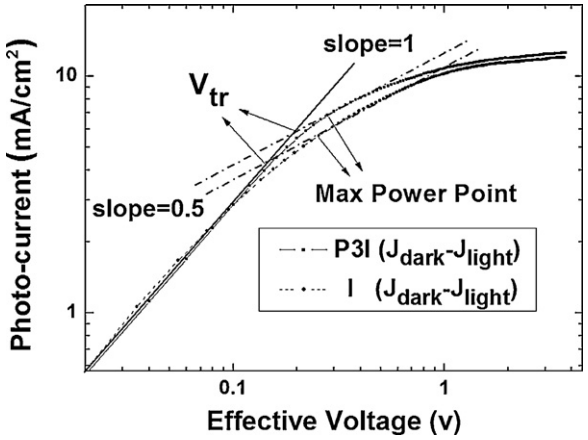

Fig. 4. The photocurrent vs. effective voltage characteristics in log–log scale.

for device P3I and I, respectively. The photo-carrier generation rate exhibits only 4.17% increase for device P3I as compared to device I, and cannot account for the 32.8% enhancement in PCE. This is again different from what was observed in Ref. [15], in which the improved PCE results mostly from increased photo-carrier generation rate.

To understand the difference between our results and Ref. [15], we estimate the charge collection length which characterizes SCL transport. Typical reported values for carrier lifetime (10 μs [17]) and hole mobility (1.5×10^{-8} m^2/V s [18]) are used and a charge collection length around 300 nm at 0.6 V was obtained for P3HT:PCBM BHJ PSCs. While this estimated value is close to the active layer thickness in our devices, it is significantly larger than that (175 nm) in Ref. [15]. The device in Ref. [15] operates therefore in the linear region and the improvement in PCE results mostly from increased photo-carrier generation rate. On the other hand, our devices employ much thicker active layers and the enhancement in PCE with inserted P3HT-rich layer arises from reduced SCL effects.

It is remarkable that the transition from the balanced transport region to the SCL region is determined by the transition voltage V_{tr} given in Eq. (2). An increased value of b in Eq. (2) leads to a larger V_{tr}, extends the linear region and thus increases the PCE and FF. From Fig. 4, V_{tr} increases by 34.8% from 0.155 to 0.209 V. This increase in V_{tr} is tentatively attributed to the increase in the effective carrier lifetime due to reduced recombination. Assumed that $\tau_f \upsilon_f$, the product of carrier mobility and lifetime of the fast carriers which are electrons in our case, remains unchanged and $b \ll 1$, V_{tr} in Eq. (2) depends linearly on b. Therefore, a rough estimate of 34.8% increase in b with the insertion of the P3HT-rich layer can be obtained.

To further investigate the effects of the inserted P3HT-rich layer on SCL transport, the short-circuit current densities under different illumination levels were measured and the results were plotted in log–log scale in Fig. 5. As shown in Fig. 5, device I exhibits a power dependence of 0.72 ± 0.04, which is close to the predicted value of 0.75 for SCL photocurrent [7]. On the other hand, an exponent of 0.94 ± 0.06 was obtained for device P3I, indicating alleviated SCL effects. This result is consistent with the observation in Fig. 5, corroborating that the insertion of P3HT-rich layer reduces SCL effects.

The IPCE of device I and P3I with and without a one-sun DC light bias were plotted in Fig. 6(a) and (b). Since both devices exhibit nearly identical absorption (Fig. 2), enhanced quantum efficiency observed in device P3I, as compared to device I, indicates improved charge collection efficiency. It is also interesting to note that the

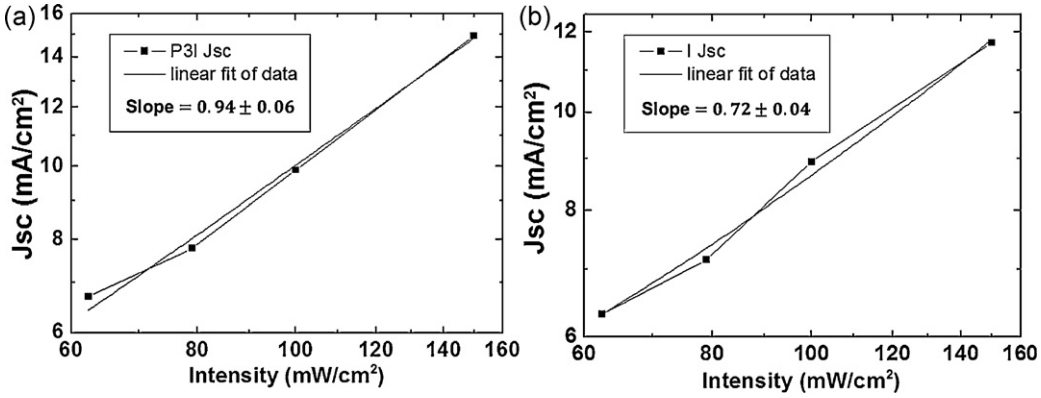

Fig. 5. The short-circuit current density vs. incident light intensity in log-log scale for (a) device P3I and (b) device I.

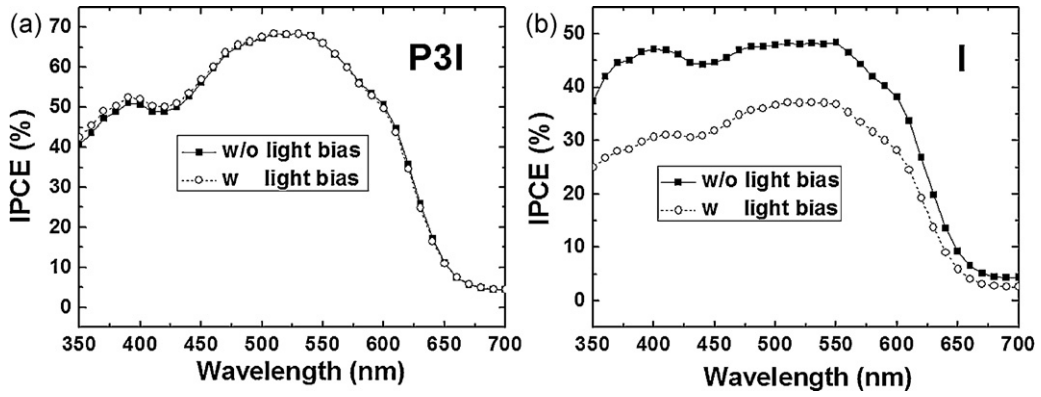

Fig. 6. Incident photon-to-electron conversion efficiency spectra with and without one-sun DC light bias for (a) device P3I and (b) device I.

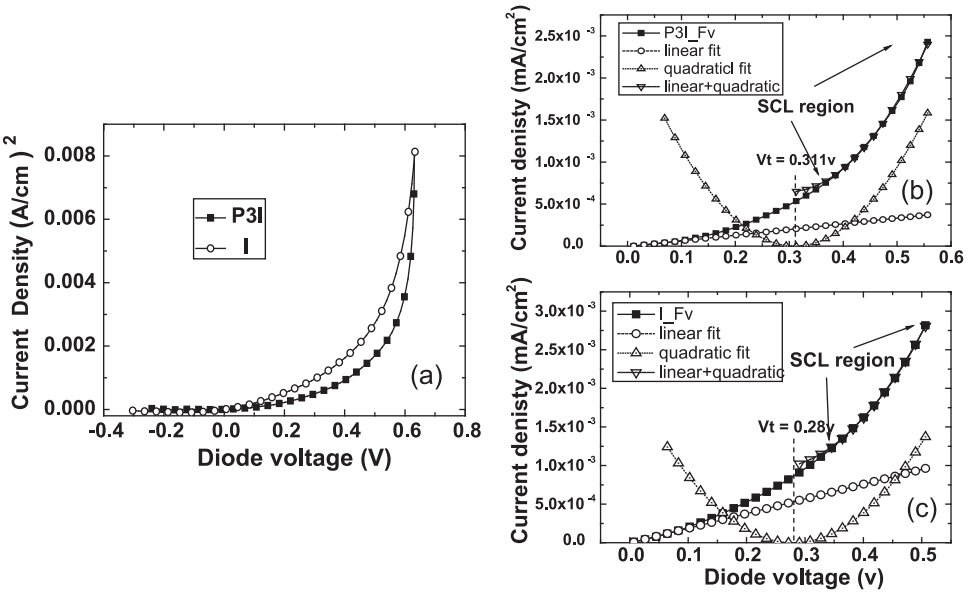

Fig. 7. (a) Extracted intrinsic *J–V* curves for device I (open circle) and P3I (solid square); extracted *J–V* curves and its decomposition into a linear and a shifted quadratic component for (b) device P3I and (c) device I. In (b) and (c) a vertical dashed line was shown to denote the shifted (transition) voltage, larger than which the quadratic SCL current takes effect.

Table 2
The extracted parameters including R_s, R_{sh} and J_{ph} for devices P3I and I.

	R_s (Ω cm^2)	R_{sh} (Ω cm^2)	J_{ph} (mA/cm^2)
P3I	14.6	407	10.4
I	9.26	312	9.44

IPCE for device I shows much stronger dependence on the DC light bias than device P3I. This can be understood by noting that the DC light bias contributes more background carriers which lead to segregated charge distribution near both sides in the devices. This charge segregation can screen the electric field in the bulk region. For devices with dominant SCL transport, such as device I, reduced electric field in the bulk region leads to decreased collection efficiency, and thus decreased IPCE. On the other hand, since the SCL effects in device P3I are already much reduced, little change in IPCE was observed with DC light bias.

Although the contacts to the active layer are crucial to the carrier extraction as well as injection [13] and affect in turn the carrier concentration within the active layer, SCL effects are intrinsically bulk effects with which the space charge modulates the bulk electric field. It would therefore be revealing to remove the effects due to the contacts, which manifest mostly as parasitic series resistance, and to study the intrinsic current–voltage (*I–V*) characteristic of the devices. We followed a procedure which we proposed previously for extracting the intrinsic *I–V* characteristics and the series resistance without assuming the *I–V* functional form [19]. In short, the extracted *I–V* represents the best fit bulk *I–V* relationship, assuming constant Ohmic (linear) *I–V* characteristic for the contacts. The procedure requires *I–V* measurements with two slightly different light illumination levels. Besides the ones with a calibrated solar simulator at AM1.5G (100 mW/cm^2), the other *I–V* curves were obtained with a microscope cover glass placed on top of the OSCs, leading to a light attenuation of about 8%. The root-mean-square error is calculated for the range from $V_D = 0$ to open-circuit voltage (V_{oc}) in the measured *I–V* characteristic with less light illumination. The detailed calculation procedure can be found in [19].

The extracted parameters including series resistance (R_s), shunt resistance (R_{sh}) and photo-induced current density (J_{ph}) were summarized in Table 2. Apparently, the R_{sh} of device P3I is increased as compared to that of device I, indicating reduced recombination of photo-carriers with the insertion of the P3HT-rich layer.

Fig. 7(a) shows the extracted intrinsic *J–V* curves for both devices. As it was shown in [19] that the intrinsic current density of OSCs at low forward bias comprises of a linear and a quadratic component, which were tentatively attributed to hopping and SCL, respectively, we subtract the linear component from the extracted *J–V* and fit the subtracted *J–V* with a shifted quadratic term around the voltage that corresponds to V_{max}; the results were shown in Fig. 7(b) and (c) for device P3I and I, respectively. From Fig. 7(b) and (c), it was clear that SCL effects appear at lower bias for device I than device P3I. It is also understandable that both voltages are larger than those obtained previously from the measured *I–V* curves, since a negative voltage drop develops across Rs with the extracted photocurrent for the measured *I–V*.

5. Conclusion

In summary, our results demonstrated that by tailoring the compositional profile of blend layer with an inserted P3HT-rich layer, the effective carrier lifetime can be increased and the detrimental SCL effects can be alleviated. With our results, it is expected that the addition of interlayers, preferably with higher carrier mobility for better carrier extraction and with less heterojunction and/or larger barrier to reduce the carrier concentration of the other type to reduce recombination, between the active layer and the electrodes will enhance the FF. It is therefore possible to increase the FF and the PCE for devices with a thick active layer with a suitably designed vertical composition profile or layer structure. Our results also show that DC light bias is important to characterize the operating characteristics of PSCs when SCL effects dominate photo-carrier carrier transport near the operating points.

Acknowledgment

This work was supported by the National Science Council (NSC) of Taiwan, ROC, under grant NSC 100-2221-E-007-079-MY3.

References

[1] F.C. Krebs, Solar Energy Materials and Solar Cells 93 (2009) 394.
[2] F.C. Krebs, M. Jørgensen, K. Norrman, O. Hagemann, J. Alstrup, T.D. Nielsen, J. Fyenbo, K. Larsen, J. Kristensen, Solar Energy Materials and Solar Cells 93 (2009) 422.
[3] G. Li, V. Shrotriya, J. Huang, Y. Yao, T. Moriarty, K. Emery, Y. Yang, Nature Materials 4 (2005) 864.
[4] W. Ma, C. Yang, X. Gong, K. Lee, A.J. Heeger, Advanced Functional Materials 15 (2005) 1617.
[5] A.J. Moulé, K. Meerholz, Advanced Materials 20 (2008) 240.
[6] J. Xue, B.P. Rand, S. Uchida, S.R. Forrest, Journal of Applied Physics 98 (2005) 124903.
[7] A.M. Goodman, A. Rose, Journal of Applied Physics 42 (1971) 2823.
[8] J. Peet, J.Y. Kim, N.E. Coates, W.L. Ma, D. Moses, A.J. Heeger, G.C. Bazan, Nature Materials 6 (2007) 497.
[9] Y.M. Chang, L. Wang, Journal of Physical Chemistry C 112 (2008) 17716.
[10] M. Canpoy-Quiles, T. Ferenczi, T. Agostinelli, P.G. Etchegoin, Y. Kim, T.D. Anthopoulos, P.N. Stavrinou, D.D.C. Bradley, J. Nelson, Nature Materials 7 (2008) 158.
[11] S. Fabiano, Z. Chen, S. Vahedi, A. Facchetti, B. Pignataroc, M.A. Loi, Journal of Materials Chemistry 21 (2011) 5891.
[12] J. Wagner, M. Gruber, A. Hinderhofer, A. Wilke, B. Bröker, J. Frisch, P. Amsalem, A. Vollmer, A. Opitz, N. Koch, F. Schreiber, W. Brütting, Advanced Functional Materials 20 (2010) 4295.
[13] Z. He, C. Zhong, X. Huang, W.Y. Wong, H. Wu, L. Chen, S. Su, Y. Cao, Advanced Materials 22 (2011) 4636.
[14] V.D. Mihailetchi, L.J.A. Koster, J.C. Hummelen, P.W.M. Blom, Physical Review Letters 93 (2004) 216601–216611.
[15] C.W. Liang, W.F. Su, L. Wang, Applied Physics Letters 95 (2009) 133303.
[16] S.R. Tseng, S.C. Lin, H.F.M. Meng, H.H. Liao, C.H. Yeh, H.C. Lai, S.F. Horng, C.S. Hsu, Applied Physics Letters 88 (2006) 163501.
[17] G.G. Belmonte, P.P. Boix, J. Bisquert, M. Sessolo, H.J. Bolink, Solar Energy Materials and Solar Cells 94 (2010) 366.
[18] L.J.A. Koster, V.D. Mihailetchi, P.W.M. Blom, Applied Physics Letters 88 (2006) 093511.
[19] M.K. Lee, J.C. Wang, S.F. Horng, H.S. Meng, Solar Energy Materials and Solar Cells 94 (2010) 578.